A Miniature Electrical Impedance Tomography Sensor and 3-D Image Reconstruction for Cell Imaging

A Miniature Electrical Impedance Tomography Sensor and 3D Image Reconstruction for Cell Imaging

Yunjie Yang, *Member, IEEE*, Jiabin Jia*, *Member, IEEE*, Stewart Smith, *Senior Member, IEEE*, Nadira Jamil, Wesam Gamal, Pierre Bagnaninchi

***Abstract*— Real-time quantitative imaging is becoming highly desirable to study nondestructively the biological behavior of three dimensional cell culture systems. In this work, we investigate the feasibility of quantitative imaging/monitoring of 3D cell culture processes via Electrical Impedance Tomography (EIT), which is capable of generating conductivity images in a non-destructive manner with high temporal resolution. To this end, a planar miniature EIT sensor amenable to standard cell culture format is designed and a 3D forward model for the sensor is developed for 3D imaging. Furthermore, a novel 3D-Laplacian and sparsity joint regularization algorithm is proposed for enhanced 3D image reconstruction. Simulation phantoms with spheres at various vertical and horizontal positions were imaged for 3D performance evaluation. In addition, experiments on human breast cancer cell spheroid and a triangular breast cancer cell pellet were carried out for experimental verification. The results have shown that stable measurement on high conductive cell culture medium and significant improvement of image quality based on the proposed regularization method are achieved. It demonstrates the feasibility of using the miniature EIT sensor and 3D image reconstruction algorithm to visualize 3D cell cultures such as spheroids or artificial tissues and organs. The established work would expedite real-time quantitative imaging of 3D cell culture for assessment of cellular dynamics.**

***Index Terms*— Cell culture, electrical impedance tomography, 3D image reconstruction, miniature sensor.**

I. Introduction

CELL culture is extensively undertaken in biotechnology industry, pharmaceutical industry, as well as research laboratories. For numerous investigative purposes during bioprocesses, cells can be passaged, cultivated, transformed, and/or transplanted [1]. In each of these operations, it is necessary to understand the status of the cells in vitro. Beyond that, improvement of product quality in highly sophisticated cell-based production processes requires sensing of key process variables in real time and imposing corrective actions when necessary [2]. Compared to the conventional 2D cell culture, 3D cell culture can provide a more realistic environment for in vitro cells to model in vivo conditions. In particular, cell spheroids are regarded as a step-change in drug discovery. As a result, real-time quantitative imaging of 3D cell culture is becoming highly desirable for study of biological behavior and control of chemical environment. For example, visualization of cell adhesion, spreading, proliferation and detachment in cell cycle processes, cellular morphology and cell-drug interaction, etc. [3]. Various sensing and imaging techniques for bioprocess monitoring have been proposed and investigated in the past decades. Such techniques include electrical-based methods, i.e., impedance spectroscopy [3-7], and optical-based methods such as Raman spectroscopy [8, 9] and microscopic imaging [10]. Compared with most optical-based methods and typical electroanalytical techniques, impedance spectroscopy can provide better characterization of cellular properties [4]. However, commonly used impedance spectroscopic methods utilize two electrode systems and consequently lack spatial resolution.

Electrical Impedance Tomography (EIT) has been an emerging medical and industrial process imaging modality over the past two decades. It has the capability to, spatially and temporally, estimate the conductivity change inside the region of interest in a non-invasive manner [11-13]. To date, EIT has been successfully applied in lung ventilation imaging [14], and recently, study of fast neurological activity by EIT has also been reported in the scientific literature [15]. EIT allows non-destructive, real-time, continuous, label-free, qualitative and even quantitative visualization with spatial-temporal resolution. Such features make EIT a promising technique for cellular imaging and bioprocess monitoring, and some pioneering work from both theoretical and practical aspects has been reported recently. The effect of cell membranes on tissue admittivity was investigated and a mathematical framework regarding this issue was derived in [16]. A mathematical framework for determining the microscopic properties of the cell culture from spectral measurements was proposed in [17], while multi-frequency measurements was also demonstrated to be effective in stability and resolution improvement in EIT

Manuscript received xx, xx, xxxx. This work was partially supported by the 2015 IEEE I&M Society Graduate Fellowship Award.

Yunjie Yang and Jiabin Jia* are with the Agile Tomography Group, Institute for Digital Communications, School of Engineering, The University of Edinburgh, Edinburgh, EH9 3JL, UK (e-mail: jiabin.jia@ed.ac.uk).

Stewart Smith and Nadira Jamil are with the Institute for Bioengineering, School of Engineering, The University of Edinburgh, SMC, Alexander Crum Brown Road, Edinburgh, EH9 3FF, UK.

Wesam Gamal and Pierre Bagnaninchi are with the Centre for Regenerative Medicine, College of Medicine and Veterinary Medicine, The University of Edinburgh, Bioquarters, 5 Little France Drive, EH16 4UU, UK.

[18]. Additionally, EIT was also implemented or explored towards on-chip cellular imaging [19], single cell freezing monitoring [20] and single cell electroporation imaging [21, 22]. The abovementioned work highlights the potential of EIT for cell substrate sensing or imaging. However, most of the reported work focused on 2D cell culture imaging using a planar EIT sensor whilst based on a 2D forward model and conventional image reconstruction algorithms [3, 19]; or a typical 2D sensor with axial electrodes [20, 21]; or 3D spectroscopic scanning using a four-electrode sensor which has no spatial resolution [5].

In this paper, we design a planar miniature EIT sensor, develop a 3D forward model that accords better with electric field distribution compared with the 2D one, and propose a novel 3D-Laplacian and sparsity joint regularization algorithm for enhanced 3D cell culture imaging. The sensor is designed considering the sensing performance under real cell culture environment, i.e., the dc drift under high conductivity medium, as well as the compatibility with cell culture dish. The structure, manufacture and modelling of the sensor are demonstrated and its sensitivity is analyzed. A novel 3D-Laplacian and sparsity joint regularization algorithm is proposed for enhanced 3D imaging, while the results are compared with 3D Total Variation (3D-TV) regularization method [23]. To evaluate the performance of the planar miniature EIT sensor and the proposed 3D image reconstruction algorithm, both simulations of test phantoms and experiments of breast cancer cell are conducted.

The paper is organized accordingly: principle and image reconstruction framework of EIT are introduced in Section II. Design and analysis of the planar miniature EIT sensor are depicted in Section III. The proposed 3D image reconstruction algorithms are demonstrated in Section IV. Simulation and experiment results are in Section V. Finally, concluding remarks and future work are given in Section VI.

II. Electrical Impedance Tomography

In EIT, the relationship between the conductivity distribution σ in the sensing domain and the measured boundary voltage difference **V** is expressed as

$$\mathbf{V} = \mathbf{F}(\sigma) + \mathbf{e} \tag{1}$$

where **F** is the nonlinear forward operator and **e** is measurement noise. In practical scenarios, Eq. (1) can be linearized and formulated as

$$\mathbf{y} \approx \mathbf{J}\mathbf{x} + \mathbf{e} \tag{2}$$

where **y** is the normalized voltage measurement; **J** is the Jacobian matrix or sensitivity matrix; **x** is the conductivity vector.

To estimate the conductivity distribution from boundary voltage measurements, an inverse problem needs to be solved. The procedure is image reconstruction and can be generally formulated as the optimization problem below:

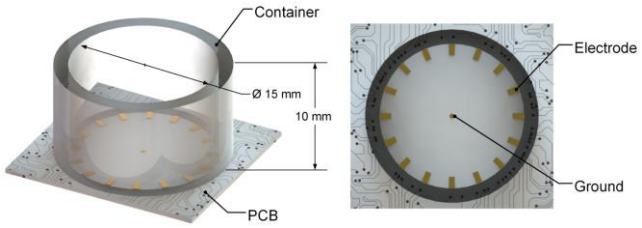

Fig. 1. Schematic illustration of designed miniature EIT sensor.

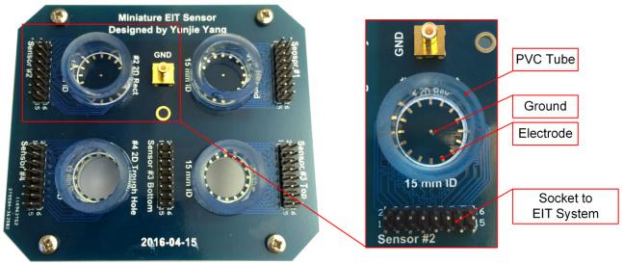

Fig. 2. Manufactured miniature EIT sensor.

$$\hat{\mathbf{x}} = \arg\min_{\mathbf{x}} \frac{1}{2}\left\|\mathbf{y} - \mathbf{J}\mathbf{x}\right\|_2^2 + \lambda \mathrm{H}(\mathbf{x}) \tag{3}$$

where $\hat{\mathbf{x}}$ denotes the estimation of conductivity distribution; H is the regularization function which incorporates the priori information and λ is the regularization factor. Tremendous progress has been made in advancing EIT image reconstruction algorithms in the past decades and comprehensive reviews can be found in [24, 25].

III. Planar Miniature EIT Sensor

A. Sensor Design

Fig. 1 shows the schematic illustration of designed miniature EIT sensor for 3D cell cultivation imaging. The sensor consists of 16 micro electrodes near the boundary of the base. This electrode configuration is adopted to easily form an appropriate cell culture dish and to avoid the noise caused by the contact impedance between the imaging target and the electrode. The inner diameter of the circular chamber is 15 mm and the height is 10 mm. The length and width of each microelectrode is 1.2 mm and 0.6 mm, respectively. All the electrodes are evenly distributed on the substrate. In addition, to reduce the DC drift of the measurement caused by the highly conductive cell culture medium, a grounded point with a diameter of 0.4 mm is added in the center of the chamber as the reference electrode. The planar electrodes configuration can generate a 3D electric field near the substrate in the axial direction, which can be used to perform subsurface imaging [26].

The planar miniature EIT sensor is manufactured on a printed circuit board, as shown in Fig. 2. Rectangular bonding pads after gold plating are used as sensing electrodes to prevent corrosion by the solution and electrochemical reaction. The length of all traces connecting the electrodes and sensor socket is equalized to minimize the impedance difference caused by trace length discrepancy.

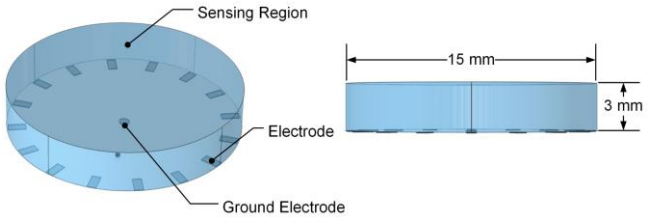

Fig. 3. The modelled planar miniature EIT sensor.

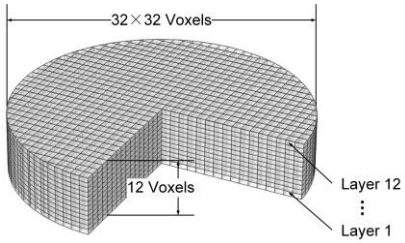

Fig. 4. Voxel mesh for inverse problem calculation.

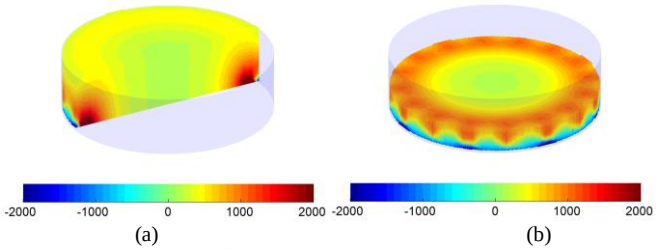

Fig. 5. The summation of the Jacobian matrix. (a) Longitudinal section. (b) Transverse section.

B. 3D Modelling and Sensitivity Analysis

The formerly reported work [19] using planar EIT sensor is based on a conventional 2D model, which does not conform to the actual situation and can introduce model error. Moreover, the 3D imaging ability is not utilized. As illustrated in Fig. 3, in this work, a 3D model of the designed planar miniature EIT sensor with culture medium is developed in COMSOL Multiphysics to reduce model error while enable 3D imaging. To be consistent with practical circumstances, the sensor model is filled up to 3 mm height with background substance. A 3D mesh for inverse problem is developed as shown in Fig. 4, where the illustrated sensing domain is longitudinally divided into 12 layers, and each layer has 32×32 voxels. As a result, the mesh is consisted of 9744 voxels in the cylindrical sensing domain. Accordingly, the 3D Jacobian matrix can be calculated by

$$\mathbf{J}_{dm}(t,z,q)=\frac{\partial \mathrm{V}_{dm}}{\partial \sigma_k}=-\int_{\text{voxel } k}\nabla \mathrm{u}_{tzq}\left(I^d\right)\cdot\nabla \mathrm{u}_{tzq}\left(I^m\right)\mathrm{dV} \quad (4)$$

where $\mathbf{J}_{dm}(t, z, q)$ is the sensitivity value at voxel (t, z, q) when electrode pairs d and m are selected as current excitation and measurement, respectively, where $1\le t\le 32$, $1\le z\le 32$, $1\le q\le 12$. $\mathrm{U}_{tzq}(I^d)$ and $\mathrm{U}_{tzq}(I^m)$ are electrical potential within the 3D sensing region when the d^{th} and m^{th} pair of electrodes are selected as current excitation electrodes, respectively. In this work, the adjacent excitation and adjacent measurement sensing protocol is applied [27], which obtains 104 independent measurements.

Fig. 5 illustrates the cross sectional distribution of the summation of the Jacobian matrix. The summation indicates the sensitivity of the designed miniature EIT sensor. The planar sensor has the largest sensitivity to at the bottom layer and decrease accordingly towards the top layers, but within the oblate sensing region, i.e., 3 mm of chamber height, the sensitivity is large enough for 3D imaging.

IV. 3D Image Reconstruction Algorithms

The conductivity distribution in the sensing region can be estimated based on the voltage measurement and the 3D Jacobian matrix in Eq. (4) using certain image reconstruction algorithms. In this section, a novel 3D-Laplacian and sparsity joint regularization algorithm is proposed for enhanced 3D imaging quality. In addition, 3D Total Variation regularization is also presented for purpose of comparison.

A. 3D-Laplacian and Sparsity Joint Regularization

A novel 3D-Laplacian and sparsity joint regularization algorithm (3D-Lap-L1) is proposed in this subsection for enhanced 3D imaging performance. Recently, sparsity constraint has been thoroughly investigated in signal and image processing field, and promising results have been demonstrated when the signal is sparse in spatial, frequency domain, or under some basis [28]. In this work, the sparsity constraint and 3D-Lapalacian operator is combined together to deal with the ill-posed 3D EIT image reconstruction problem depicted in Eq. (3). The 3D-Laplacian operator shown in Fig. (6) imposes constraint on the vertical as well as horizontal directions for enhanced 3D positioning, while the sparsity constraint introduces the sparse prior and excellent noise reduction performance. The combination of both terms exhibits the features of both terms. The algorithm is formulated as

$$\hat{\mathbf{x}}=\arg\min_{\mathbf{x}}\frac{1}{2}\left\|\mathbf{y}-\mathbf{J}\mathbf{x}\right\|_2^2+\lambda_1\left\|\mathbf{L}\mathbf{x}\right\|_2^2+\lambda_2\left\|\mathbf{x}\right\|_1 \quad (5)$$

where, $\hat{\mathbf{x}}$ denotes the estimation of the true conductivity distribution; λ_1 and λ_2 are regularization factors of the 3D-Laplacian term and the sparsity term, respectively; $\mathbf{L}$ is the 3D-Laplacian operator matrix [27], which can be calculated based on the definition illustrated in Fig. (6):

$$\mathbf{L}=\begin{bmatrix}3 & -1 & \cdots & 0\\ -1 & 6 & \cdots & 0\\ & & \ddots & \\ 0 & 0 & \cdots & 3\end{bmatrix} \quad (6)$$

Eq. (5) can be rewritten as

$$\hat{\mathbf{x}}=\arg\min_{\mathbf{x}}\frac{1}{2}\left\|\begin{bmatrix}\mathbf{y}\\ 0\end{bmatrix}-\begin{bmatrix}\mathbf{J}\\ \sqrt{\lambda_1}\mathbf{L}\end{bmatrix}\mathbf{x}\right\|_2^2+\lambda_2\left\|\mathbf{x}\right\|_1 \quad (7)$$

Eq. (6) can be further rewritten as

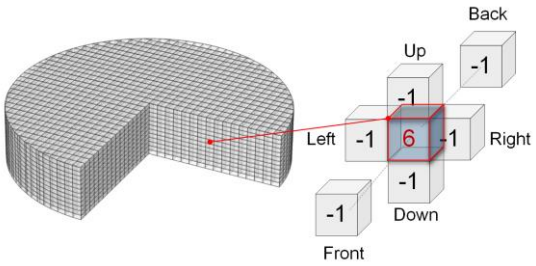

Fig. 6. 3D Laplacian operator applied to a voxel.

$$\hat{\mathbf{x}} = \arg\min_{\mathbf{x}} \frac{1}{2}\left\|\mathbf{b} - \mathbf{A}_{\lambda_1}\mathbf{x}\right\|_2^2 + \lambda_2 \left\|\mathbf{x}\right\|_1 \tag{7}$$

where

$$\mathbf{b} = \begin{bmatrix} \mathbf{y} \\ 0 \end{bmatrix},\ \mathbf{A}_{\lambda_1} = \begin{bmatrix} \mathbf{J} \\ \sqrt{\lambda_1}\mathbf{L} \end{bmatrix} \tag{8}$$

The optimization problem in Eq. (7) with nonquadratic convex regularizer is solved by a Two-step Iterative Shrinkage/Thresholding Algorithm (TwIST) [30], which exhibits fast convergence rate for ill-conditioned problems. The iteration framework of is

$$\begin{aligned} \hat{\mathbf{x}}_1 &= \Psi_\mu\left(\hat{\mathbf{x}}_0\right) \\ \hat{\mathbf{x}}_{k+1} &= \left(1-\alpha\right)\hat{\mathbf{x}}_{k-1} + \left(\alpha-\delta\right)\hat{\mathbf{x}}_k + \delta\cdot\Psi_\mu\left(\hat{\mathbf{x}}_k\right) \end{aligned} \tag{9}$$

where, $\hat{\mathbf{x}}_{k+1}$ and $\hat{\mathbf{x}}_k$ are the estimation of conductivity distribution at the k+1 and k step ($k\geq1$), respectively; $\hat{\mathbf{x}}_0$ is the initial value, which is $\hat{\mathbf{x}}_0 = (\mathbf{J}^T\mathbf{J} + \lambda\mathbf{L}^T\mathbf{L})^{-1}\mathbf{J}^T\mathbf{y}$, λ=0.0001 in this work; α, δ>0 are parameters, and

$$\Psi_\mu\left(\mathbf{x}\right) = \Gamma_\mu\left(\mathbf{x} + \mathbf{A}^T\left(\mathbf{b} - \mathbf{A}\mathbf{x}\right)\right) \tag{10}$$

where $\mu = \lambda_2$ is the regularization parameter. Γ_μ is the denoising function and in this case is the well-known soft-thresholding function [31] which is expressed as

$$\left[\cdots, sign\left(x_i\right)\max\left\{0, \left|x_i\right| - \mu\right\}, \cdots\right] = \Gamma_\mu\left(\left[\cdots, x_i, \cdots\right]\right) \tag{11}$$

where x_i is the i^{th} element of $\mathbf{x}$ and sign is the sign function.

B. 3D Total Variation Regularization

The 3D Total Variation regularization (3D-TV) [23] is also implemented for 3D image reconstruction as comparison, which is formulated as

$$\hat{\mathbf{x}} = \arg\min_{\mathbf{x}} \frac{1}{2}\left\|\mathbf{y} - \mathbf{J}\mathbf{x}\right\|_2^2 + \lambda\left\|\mathbf{x}\right\|_{\mathbf{TV}_{3D}} \tag{12}$$

where, $\hat{\mathbf{x}}$ denotes the estimation of true conductivity distribution in the sensing domain; λ is the regularization factor; $\left\|\mathbf{x}\right\|_{\mathbf{TV}_{3D}}$ is the 3D-TV norm of the conductivity distribution, which is defined as

$$\begin{aligned} \left\|\mathbf{x}\right\|_{\mathbf{TV}_{3D}} &= \sum_{m,k,l}\sqrt{\left(D^v_{m,k,l}\mathbf{x}\right)^2 + \left(D^h_{m,k,l}\mathbf{x}\right)^2 + \left(D^n_{m,k,l}\mathbf{x}\right)^2} \\ &= \sum_{m,k,l}\left|\nabla_{m,k,l}\,\mathbf{x}\right| \end{aligned} \tag{13}$$

where, $[m, k, l]$ is the coordinate of a voxel at the $N\times N\times P$ 3D conductivity image $\mathbf{x}$, with $1\leq m\leq N$, $1\leq k\leq N$ and $1\leq l\leq P$. $D^v_{m,k,l}\mathbf{x}$, $D^h_{m,k,l}\mathbf{x}$ and $D^n_{m,k,l}\mathbf{x}$ are the derivatives of $\mathbf{x}$ along vertical, horizontal and normal directions, respectively, and each can be expressed as

$$D^h_{m,k,l}\mathbf{x} = \begin{cases} \mathbf{x}_{m,k,l} - \mathbf{x}_{m+1,k,l} & 1\leq m < N \\ 0 & m = N \end{cases} \tag{14}$$

$$D^v_{m,k,l}\mathbf{x} = \begin{cases} \mathbf{x}_{m,k,l} - \mathbf{x}_{m,k+1,l} & 1\leq k < N \\ 0 & k = N \end{cases} \tag{15}$$

$$D^n_{m,k,l}\mathbf{x} = \begin{cases} \mathbf{x}_{m,k,l} - \mathbf{x}_{m,k,l+1} & 1\leq l < P \\ 0 & n = P \end{cases} \tag{16}$$

The gradient-based steepest descent method is applied to solve the optimization problem depicted in (8) iteratively [32].

V. Results and Discussion

3D image reconstructions based on simulation data and experimental data are carried out in this section to validate the performance of the miniature EIT sensor and the proposed 3D image reconstruction algorithm.

A. Results Based on Simulation Data

Six small spheroid phantoms simulating the cell spheroid along the vertical and horizontal directions were modelled in the simulation to test the 3D imaging performance. Fig. 7 shows the top view and side view of the test phantoms established in the simulation based on the sensor model depicted in Fig. 3. The material of the spheroid is Titanium beta-21S. The diameter of the spheroid is 0.55 mm and the diameter ratio regarding the sensor is 3.2%. In order to be consistent with the cell culture requirements, the background substance in simulation has the same conductivity (1.9 $S\cdot m^{-1}$) with phosphate buffer solution (PBS), which is commonly used as cell culture medium.

To quantitatively evaluate the image quality, the correlation coefficients (cc) [25] between the reconstructed conductivity distribution and the ground truth are used, which is defined as

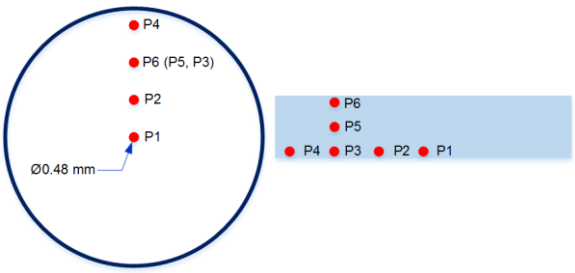

(a) (b)

Fig. 7. Spheroid phantoms used in 3D imaging tests. (a) Top view. (b) Side view.

$$CC = \frac{\sum_{i=1}^{w}\left(\hat{\mathbf{x}}_i - \bar{\hat{\mathbf{x}}}_i\right)\left(\mathbf{x}_i - \bar{\mathbf{x}}_i\right)}{\sqrt{\sum_{i=1}^{w}\left(\hat{\mathbf{x}}_i - \bar{\hat{\mathbf{x}}}_i\right)^2 \sum_{i=1}^{w}\left(\mathbf{x}_i - \bar{\mathbf{x}}_i\right)^2}} \tag{17}$$

where, $\hat{\mathbf{x}}$ and $\mathbf{x}$ denote the estimation and the true conductivity distribution in the sensing domain, respectively; $\bar{\hat{\mathbf{x}}}$ and $\bar{\mathbf{x}}$ denote the mean values of $\hat{\mathbf{x}}$ and $\mathbf{x}$, respectively. w is the total number of voxels which is 9744 in this work.

Fig. 8 to Fig. 13 show the image reconstruction results of the

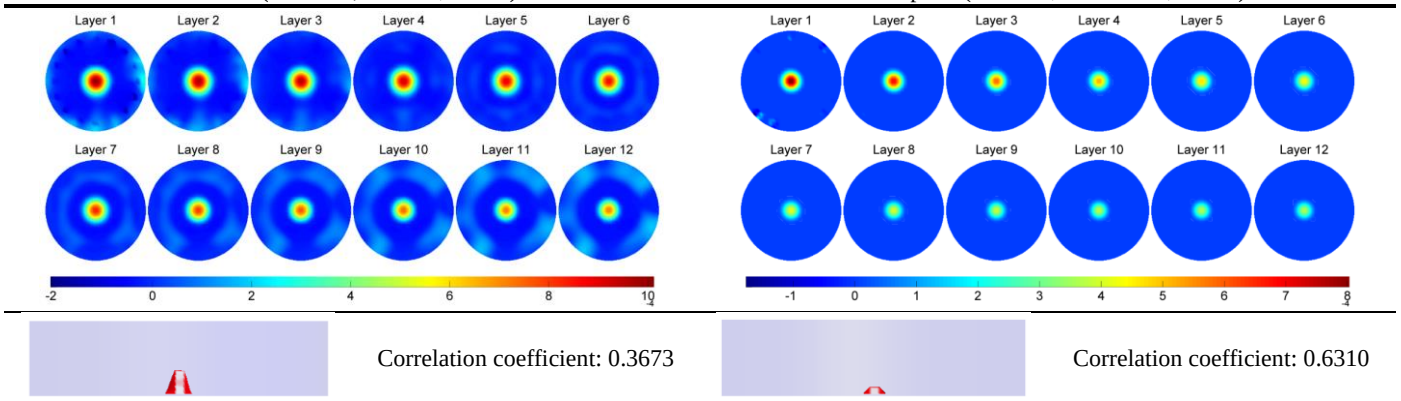

Fig. 8. Reconstructed images of spheroid phantom P1. The second row shows the sliced images of each layer the third row shows the synthesized 3D images.

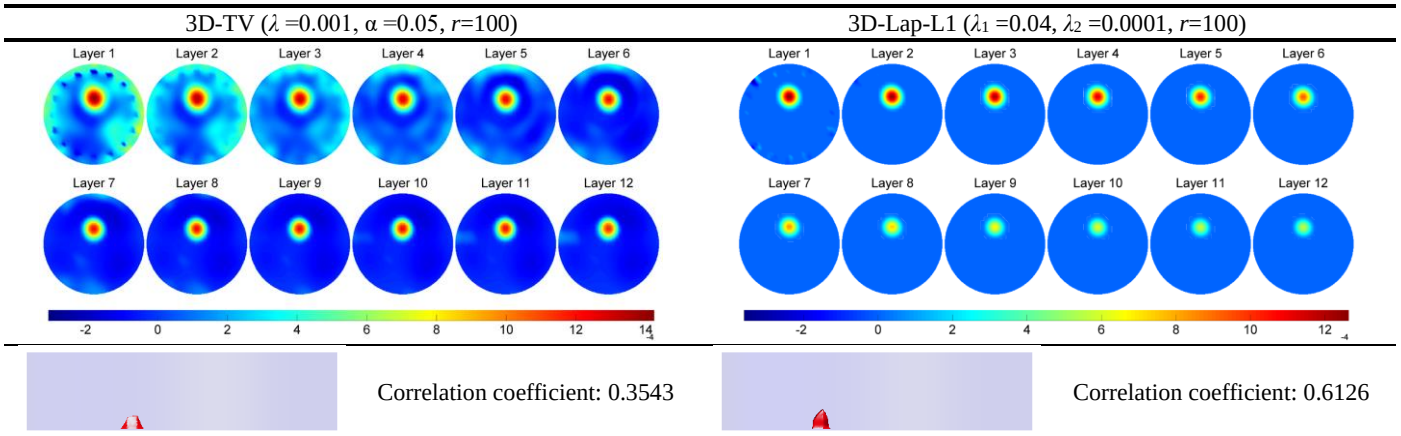

Fig. 9. Reconstructed images of spheroid phantom P2. The second row shows the sliced images of each layer the third row shows the synthesized 3D images.

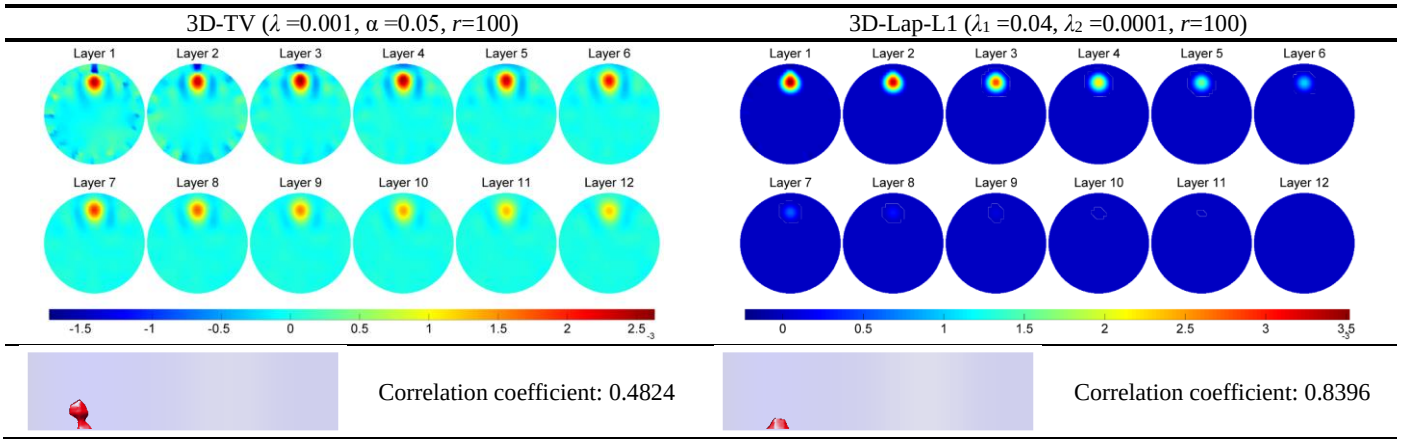

Fig. 10. Reconstructed images of spheroid phantom P3. The second row shows the sliced images of each layer the third row shows the synthesized 3D images.

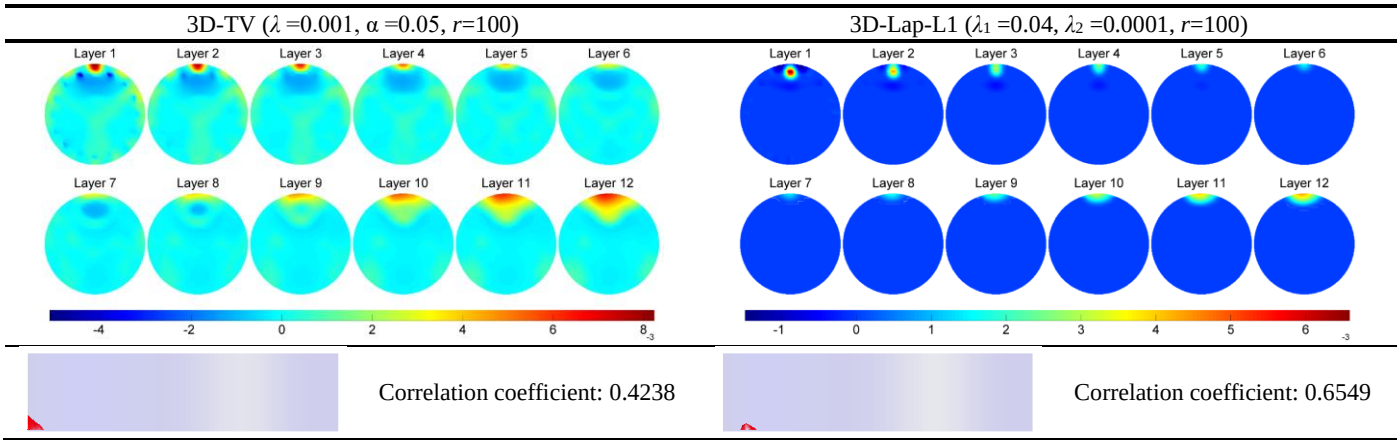

Fig. 11. Reconstructed images of spheroid phantom P4. The second row shows the sliced images of each layer the third row shows the synthesized 3D images.

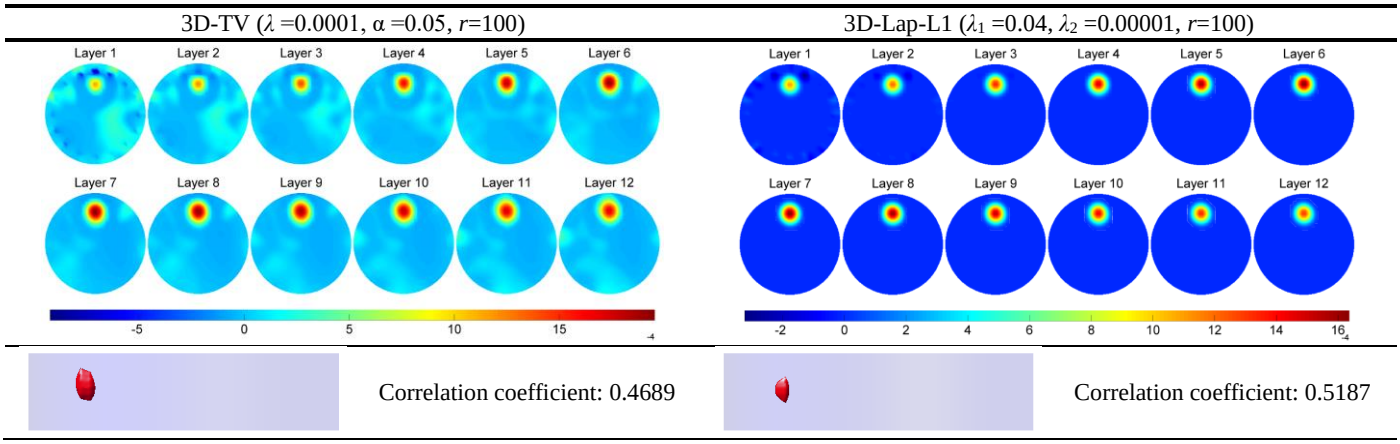

Fig. 12. Reconstructed images of spheroid phantom P5. The second row shows the sliced images of each layer the third row shows the synthesized 3D images.

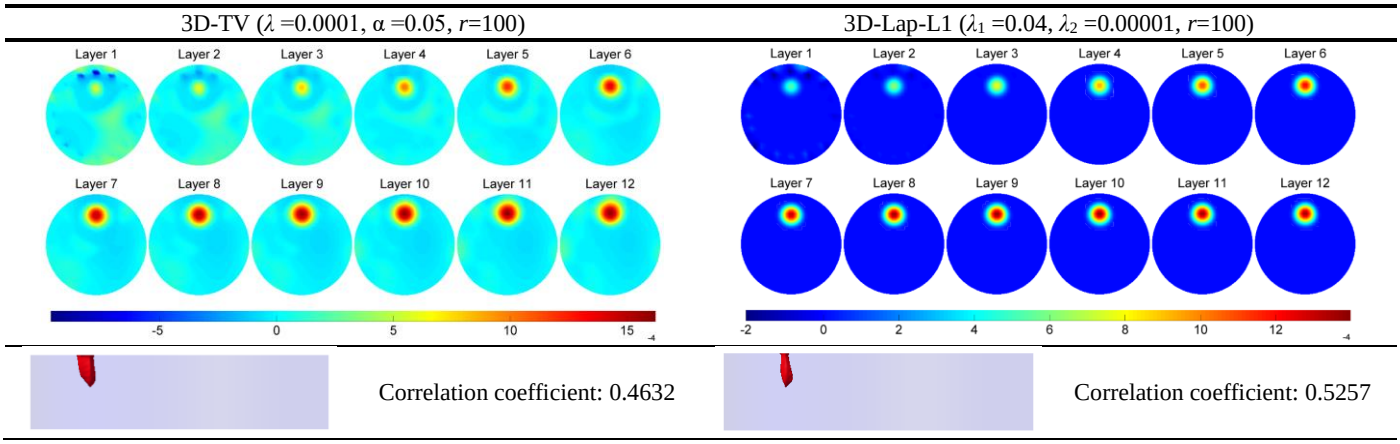

Fig. 13. Reconstructed images of spheroid phantom P6. The second row shows the sliced images of each layer the third row shows the synthesized 3D images.

six spheroid phantoms, P1 to P6, using the proposed 3D-Laplacian and sparsity joint regularization (3D-Lap-L1) and the 3D-TV regularization algorithms. The parameters used in the algorithms, such as the regularization factor λ, iteration step factor α and maximum iteration number r are also illustrated in the corresponding figures. Both sliced images of each layer and synthesized 3D images are presented in each figure. In sliced images, layer 1 corresponds to the bottom layer in Fig. 4, and in sequence, layer 12 corresponds to the top layer in Fig. 4. The synthesized 3D image is the superposition of each layer and scatter interpolation is applied between layers to achieve smooth illustration. In order to visualize the object more vividly, the isosurface of 90% maximum and minimum conductivity value in the synthesized 3D images are shown.

The simulation results indicate that the planar miniature EIT sensor with the presented algorithms can correctly estimate the conductivity changes at the vertical and horizontal directions in the 3D sensing domain. Comparing the results, the proposed 3D-Lap-L1 algorithm demonstrates superior image quality, noise reduction performance as well as location estimation result. The results using 3D-Lap-L1 also have higher correlation coefficients compared with those using 3D-TV.

B. *Results Based on Experimental Data*

Cell culture imaging using EIT is challenging due to the small scale of the sensor and highly conductive culture medium (approximately 2.0 $S \cdot m^{-1}$ or higher). In this section, static imaging on breast cancer cell spheroids and triangular pellet were carried out to validate the performance of the designed sensor and the proposed 3D image reconstruction algorithm.

A flexible, high speed, multi-frequency EIT system in compliance with medical standard (class II, BF type) was developed in the agile tomography group in the University of Edinburgh for real-time 3D biomedical imaging [33]. The EIT system with the manufactured miniature EIT sensor are shown in Fig. 14.

In experiments, the cell culture medium, PBS, is used as background substance. The conductivity of PBS is 1.9 $S \cdot m^{-1}$. The frequency of current excitation is 10 kHz and the amplitude of current is approximately 1.5 mA peak to peak. The height of PBS is 3 mm. The maximum signal to noise ratio (SNR) is 73.09 dB and the minimum SNR is 55.18 dB among all measurement channels on the designed miniature sensor with pure background substance.

Two experiment phantoms, i.e., a human breast cancer cell spheroid and a high-density triangular breast cancer cell pellet, are tested; see Fig. 15(b) and Fig. 15(c), respectively. The diameter of the cell spheroid is approximately 0.55 mm. Fig. 15(a) also shows the microscope image of the cell spheroid used in the experiment. For practical reason, i.e. to remove cell pellet from centrifuge tube, we cast a 1% agarose gel on top, and as a result, part of the cell pellet was attached to the gel but not mixed together. Gel (agarose) was made with PBS which was the same with the background substance and was seen as transparent by the EIT system.

The measured voltage on each electrode pairs, the sliced reconstruction results of each layer, and the synthesized 3D images of the two tested phantoms are demonstrated in Fig. 16 and Fig. 17, respectively. Algorithm parameters used in the procedures are presented in the figures as well.

As for the phantom 1 in Fig. 16, the diameter ratio of the spheroid and the sensor is 3.7%, making the measurement and reconstruction challenging. The measured voltage change is smaller than 2% as can be seen from Fig. 16. The reconstruction results using the proposed algorithm, i.e., 3D-Lap-L1, show correct position and superior noise reduction performance compared with the 3D-TV algorithm.

As for the phantom 2 in Fig. 17, the length of the trilateral is around 4.2 mm, 3.6 mm, and 4.5 mm, respectively. The measured voltage change is smaller than 5% as can be seen from Fig. 17. It is shown in the sliced images that the proposed 3D-Lap-L1 demonstrates much less noise near the bottom of the sensor compared with the 3D-TV algorithm. Furthermore, the 3D-Lap-L1 shows better 3D imaging ability on the vertical direction compared with the 3D-TV. Overall, significant improvement of image quality can be obtained via using the proposed 3D-Lap-L1 algorithm.

The experiment results verify the feasibility of using the designed miniature EIT sensor and 3D algorithms for cellular imaging.

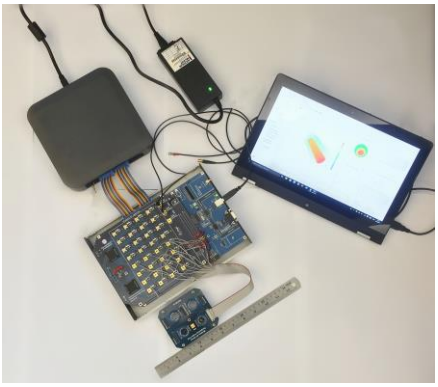

Fig. 14. The EIT system and sensor used in cell imaging experiments.

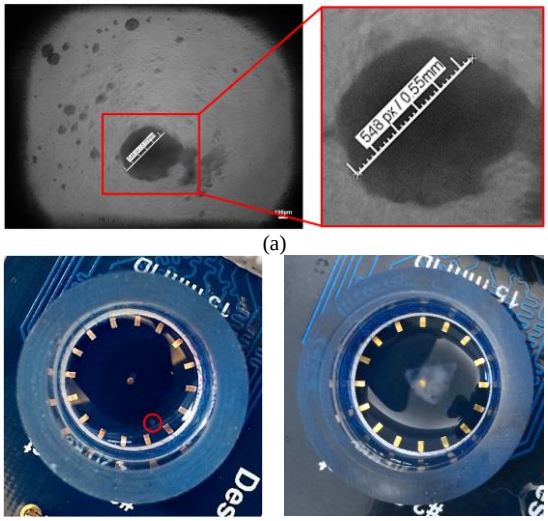

(a) (b) (c)

Fig. 15. The experiment phantoms. (a) Microscope image of the cell spheroid. (b) Phantom 1: cell spheroid with 0.55 mm diameter. (c) Phantom 2: triangular cell pellet.

VI. Conclusions

In this paper, we focus on the systematic study of applying EIT to quantitatively image and monitor 3D cell culture systems. We designed a planar miniature EIT sensor for subsurface imaging, proposed a novel 3D image reconstruction algorithm, and evaluated the simulation and experimental studies at the end. A novel 3D-Laplacian and sparsity joint regularization algorithm was proposed for enhanced 3D imaging while a 3D Total Variation regularization algorithm was applied for comparison. Simulation has shown that the planar miniature EIT sensor can measure the voltage changes induced by conductivity changes at horizontal and vertical positions. Furthermore, the sensor and proposed image reconstruction algorithm were tested using the EIT system developed in our research group. A breast cancer cell spheroid and a triangular cancer cell pellet were imaged, reconstructed, and analyzed. Both simulation and experiment results confirm the improvement of image quality using the proposed algorithm. In conclusion, we have shown that the designed planar miniature EIT sensor together with the proposed 3D image reconstruction algorithm can produce stable, high quality images for 3D cellular substance imaging and

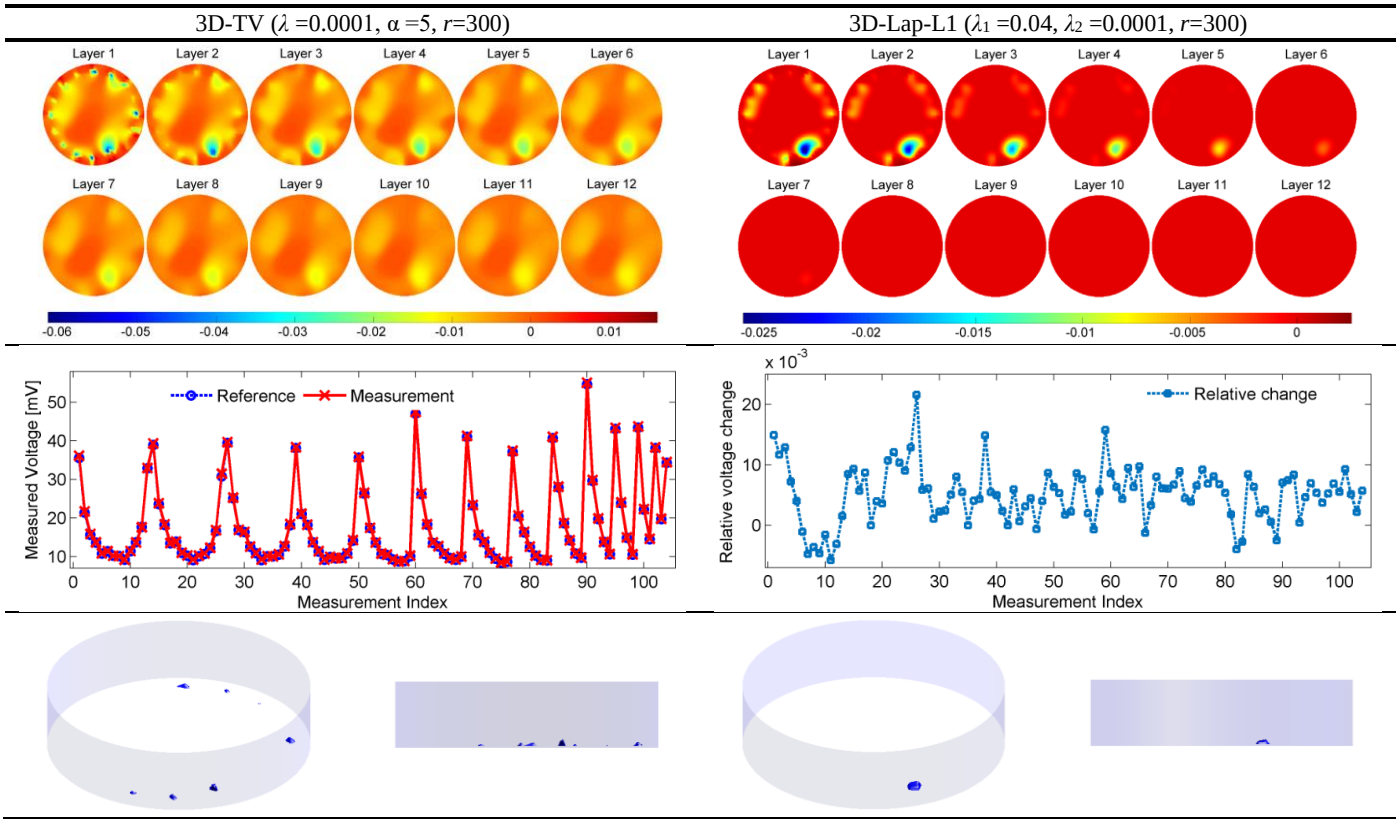

Fig. 16. Reconstructed images of cell spheroid, phantom 1. The first row shows the sliced images of each layer; the second row shows the measurement voltage and relative voltage change; the third row shows the synthesized 3D images.

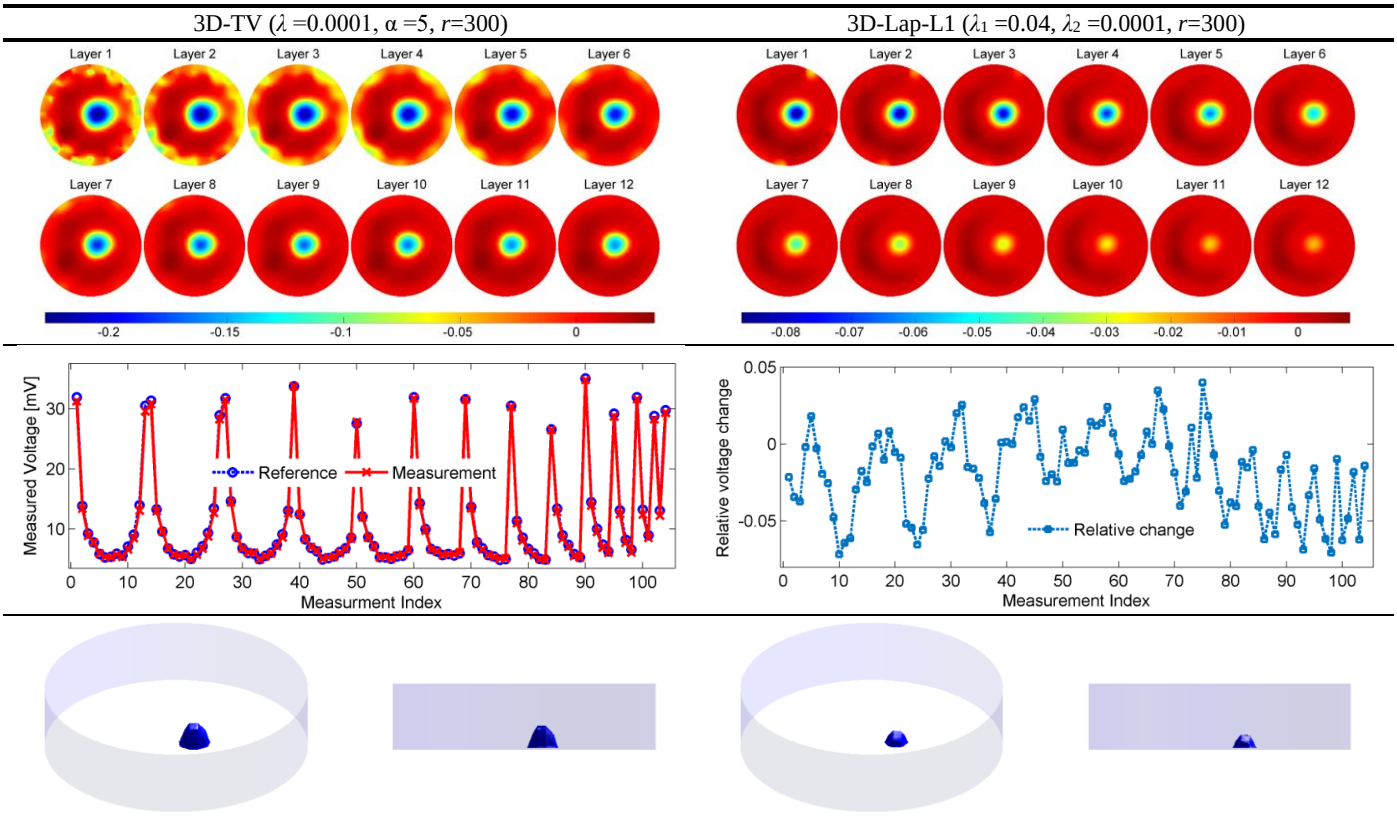

Fig. 17. Reconstructed images of triangular cell pellet, phantom 2. The first row shows the sliced images of each layer; the second row shows the measurement voltage and relative voltage change; the third row shows the synthesized 3D images.

monitoring. The high image quality while imaging small scale cell spheroids can ensure more reliable and accurate analysis of the cell-drug interaction process in the further study.

Future work will focus on the optimization of the sensor

dimension and structure, manufacture of the sensor using advanced manufacture technique, study of multi-frequency cell culture imaging and real-time quantitative imaging of 3D cell culture for the assessment of dynamics such as cell adhesion, proliferation, differentiation and cell-drug interaction.

ACKNOWLEDGMENT

The work is partly supported by 2015 IEEE Instrumentation & Measurement Society Graduate Fellowship Award.

REFERENCES

[1] W. D. Peterson Jr et al., "Cell culture characterization: monitoring for cell identification," *Methods in enzymology*, vol. 58, pp. 164–178, 1978.
[2] L. Zhao et al., "Advances in process monitoring tools for cell culture bioprocesses," *Engineering in Life Sciences*, vol. 15, no. 5, pp. 459–468, 2015.
[3] A. R. A. Rahman et al., "Cell culture monitoring by impedance mapping using a multielectrode scanning impedance spectroscopy system (CellMap)," *Physiological measurement*, vol. 29, no. 6, S227, 2008.
[4] I. O. K'Owino et al., "Impedance spectroscopy: a powerful tool for rapid biomolecular screening and cell culture monitoring," *Electroanalysis*, vol. 17, no. 23, pp. 2101–2113, 2005.
[5] C. Canali et al., "Bioimpedance monitoring of 3D cell culturing–Complementary electrode configurations for enhanced spatial sensitivity," *Biosensors and Bioelectronics*, vol. 63, pp. 72–79, 2015.
[6] P. O. Bagnaninchi et al., "Real-time label-free monitoring of adipose-derived stem cell differentiation with electric cell-substrate impedance sensing," *Proceedings of the National Academy of Sciences*, vol. 108, no. 16, pp. 6462–6467, 2011.
[7] C. Holmes et al., "Polyelectrolyte Multilayer Coating of 3D Scaffolds Enhances Tissue Growth and Gene Delivery: Non-Invasive and Label-Free Assessment," *Advanced healthcare materials*, vol. 3, no. 4, pp. 572–580, 2014.
[8] N. R. Abu-Absi et al, "Real time monitoring of multiple parameters in mammalian cell culture bioreactors using an in-line Raman spectroscopy probe," *Biotechnology and bioengineering*, vol. 108, no. 5, pp. 1215–1221, 2011.
[9] R. Mouras et al., "Multimodal, label‐free nonlinear optical imaging for applications in biology and biomedical science," *Journal of Raman Spectroscopy*, vol. 44, no. 10, pp. 1373–1378, 2013.
[10] J. S. Guez et al., "Real time in situ microscopy for animal cell-concentration monitoring during high density culture in bioreactor," *Journal of biotechnology*, vol. 111, no.3, pp. 335–343, 2004.
[11] L. Borcea, "Electrical impedance tomography," *Inverse problems*, vol. 18, no.6, R99, 2002.
[12] T. A. York, et al., "Towards process tomography for monitoring pressure filtration," *IEEE Sensors Journal*, vol. 5, no. 2, pp. 139–152, 2005.
[13] B. R. Loyola et al., "Spatial sensing using electrical impedance tomography," *IEEE Sensors Journal*, vol. 13, no. 6, pp. 2357–2367, 2013.
[14] I. Frerichs, "Electrical impedance tomography (EIT) in applications related to lung and ventilation: a review of experimental and clinical activities," *Physiological measurement*, vol. 21, no.2, R1, 2000.
[15] K. Y. Aristovich et al., "Imaging fast electrical activity in the brain with electrical impedance tomography," *NeuroImage*, vol. 124, pp. 204–213, 2016.
[16] H. Ammari et al., "Spectroscopic imaging of a dilute cell suspension," *Journal de Mathématiques Pures et Appliquées*, vol. 105, no. 5, pp. 603–661.
[17] H. Ammari et al., "Spectroscopic conductivity imaging of a cell culture," *Asymptotic Analysis*, vol. 100, no. 1–2, pp. 87–109, 2016.
[18] B. Jin et al., "The Linearized Inverse Problem in Multifrequency Electrical Impedance Tomography," *SIAM Journal on Imaging Sciences*, 2016, in press.
[19] T. Sun et al., "On-chip electrical impedance tomography for imaging biological cells," *Biosensors and Bioelectronics*, vol. 25, no .5, pp. 1109–1115, 2010.
[20] T. Hiraga et al., "Basic study on visualization of a cell during freezing using electrical impedance tomography," *Transactions of Japanese Society for Medical and Biological Engineering*, vol. 51.Supplement, R-253, 2013.
[21] A. Meir et al., "Electrical impedance tomographic imaging of a single cell electroporation," *Biomedical microdevices*, vol. 16, no. 3, pp. 427–437, 2014.
[22] H. Ammari et al., "Towards monitoring critical microscopic parameters for electropermeabilization," *Quarterly of Applied Mathematics*, 2016.
[23] M. Ertas et al., "Digital breast tomosynthesis image reconstruction using 2D and 3D total variation minimization," *Biomed Eng Online*, vo. 12, no. 112, pp. 10–1186, 2013.
[24] W. R. B. Lionheart, "EIT reconstruction algorithms: pitfalls, challenges and recent developments," *Physiological measurement*, vol. 25, no. 1, p. 125, 2004.
[25] W. Q. Yang et al., "Image reconstruction algorithms for electrical capacitance tomography," *Measurement Science and Technology*, vol. 14, no. 1, R1, 2002.
[26] X. Hu et al., "Planar capacitive sensors-designs and applications," *Sensor Review*, vol. 30, no. 1, pp. 24–39, 2010.
[27] B. H. Brown et al., "The Sheffield data collection system," *Clinical Physics and Physiological Measurement*, vol. 8, no. 4A, p. 91, 1987.
[28] E. Candes et al., "Sparsity and incoherence in compressive sampling," *Inverse problems*, vol. 23, no. 3, p. 969, 2007.
[29] Y. Yang et al., "Effect of structured packing on EIT image reconstruction," in *Proc. IEEE International Conference on Imaging Systems and Techniques*, 2014, pp. 53–58.
[30] J. M. Bioucas-Dias et al., "A new TwIST: two-step iterative shrinkage/thresholding algorithms for image restoration," *IEEE Transactions on Image processing*, vol. 16, no. 12, pp. 2992–3004, 2007.
[31] D. L. Donoho, "De-noising by soft-thresholding," *IEEE transactions on information theory*, vol. 41, no. 3, pp. 613–627, 1995.
[32] Y. Yang et al., "Data pattern with ECT sensor and its impact on image reconstruction," *IEEE Sensors Journal*, vol. 13.5, pp. 1582–1593, 2013.
[33] Y. Yang et al., "A flexible multi-frequency electrical impedance tomography system for real-time 3D biomedical imaging," 2016, unpublished.

Yunjie Yang (M'13) received the B.Eng.(hons) and M.Sc.(hons) degrees in measurement & control engineering at Anhui University, China, in 2010, and Tsinghua University, China, in 2013, respectively. Currently he is a PhD candidate with the Agile Tomography Group, School of Engineering, University of Edinburgh, UK. His current research interest includes Electrical Impedance Tomography and Electrical Capacitance Tomography for biomedical and industrial imaging. He is the recipient of 2015 IEEE I&M Society Graduate Fellowship Award.

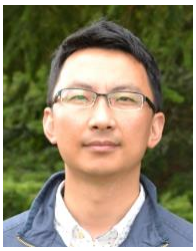

Jiabin Jia (M'15) was born in Inner Mongolia, China, in 1980. He received the B.Eng. and Master degree in Electrical and Electronics Engineering from the Wuhan University, China, in 2002 and 2005 respectively. After working for one year in H3C Technology Co., Ltd as a hardware engineer, he started his PhD study at the University of Leeds supported by the Overseas Research Students Award Scheme Award in 2006 and completed in 2010. Then he was a Research Fellow and worked on an EPSRC project for three years. In October 2013, he was appointed as a Lecturer in the School of Engineering, the University of Edinburg. His current research interests include electrical tomography, multiphase flow measurement, instruement development and medical imaging.

Stewart Smith (SM'12) received the B.Eng.(hons) degree in electronics and electrical engineering in 1997 and the Ph.D. degree in 2003 from the University of Edinburgh, Scotland, UK. He is currently a lecturer in the School of Engineering at the University of Edinburgh and a member of the Research Institute for Bioengineering. Stewart is a member of the technical committee for the IEEE International Conference on Microelectronic Test Structures and an officer of the Scottish Chapter of the IEEE Electron Devices Society. His current research focus includes the design and fabrication of bioelectronic and biomedical microsystems, microfluidics and biosensors, and development of test structures for MEMS and microsystems processes.

Nadira Jamil is a PhD student at the Institute for Bioengineering, University of Edinburgh. Her current research project focuses on microelectrodes design and fabrication for electrical impedance tomography of 3D cell cultures. She received the B.Eng and M.Sc degrees in Electronics Engineering from International Islamic University Malaysia, in 2008 and 2013 respectively. She joined Texas Instruments (TI) Malaysia in 2008 where she was involved with fab automation systems and analogue devices' characterization. In 2011, she joined Infineon Technologies (Malaysia) as a Product Development Engineer. She is a Graduate Member of the Board of Engineers Malaysia and Institute of Electrical and Electronics Engineers.

Wesam Gamal has obtained her PhD in bioengineering in 2016 from the University of Edinburgh, United Kingdom. She then worked as a post-doctoral research assistant in the lab of Dr Pierre Bagnaninchi at the MRC Centre for Regenerative Medicine. Working as part of the UKRMP hub in engineering and exploiting the stem cell niche, she studied the physical properties of stem and cancer cells (mechanical and electrical) using digital holography and OCT. Her research interests lie within developing non-invasive platforms for quantitative monitoring of cellular behavior and disease mechanisms in real-time. She is also interested in investigating the therapeutic potential of externally applied electrical fields (electrical stimulation) on wound healing and cell migration.

Pierre-Olivier Bagnaninchi is a principal investigator at the College of Medicine and Veterinary Medicine (CMVM), at the University of Edinburgh (UoE), affiliated to the MRC Centre for Regenerative Medicine. Pierre-Olivier studied theoretical physics (MSc, 97) before moving to the field of biomedical engineering. He obtained his PhD in biomedical engineering in 2001 from the University of Grenoble, France in partnership with Thales. He then accepted a two-year post-doctoral position at McGill University in Prof. Maryam Tabrizian lab to develop biosensors for tissue engineering applications. In 2004, he joined as a post-doctoral research associate the Institute of Science and Technology for Medicine at Keele University (UK) under the supervision of Prof. Alicia El Haj to conduct research on optical coherence tomography. In 2008 he was awarded a prestigious RCUK fellowship at the University of Edinburgh, where he has been appointed principal investigator in 2013. His research is currently focused on developing real-time non-invasive monitoring technologies for tissue engineering and regenerative medicine (TERM), exploiting impedance spectroscopy and optical coherence tomography, and their combination to quantitatively monitor cell proliferation and differentiation in 2D and 3D cultures.